Carbon-doped anatase titania nanoparticles: similarities and differences with respect to bulk and extended surface models

Elena R. Remesal, Ángel Morales-García*

Departament de Ciència de Materials i Química Física & Institut de Química Teòrica i Computacional (IQTCUB), Universitat de Barcelona, c/ Martí i Franquès 1-11, 08028 Barcelona, Spain

e-mail: angel.morales@ub.edu

Abstract

C-doping in titania nanoparticles is analyzed by using all electron density functional theory-based calculations considering the $(TiO_2)_{84}$ nanoparticle as a realistic representative of nanoparticles in the scalable regime. Several sites are evaluated including substituting oxygen (C_O) and titanium (C_{Ti}) sites as well as interstitial (C_i) situations. The formation energy of such doped structure is studied as a function of the oxygen chemical potential (or oxygen partial pressure). Our calculations predict that low partial oxygen pressure favors the formation of C-doped $(TiO_2)_{84}$ NP at oxygen and interstitial sites. For the former the most stable situation is for O sites at the inner part of the nanoparticle. Interestingly, the substitution of O by C at facet sites requires formation energies as those reported in previous studies where bulk anatase and surfaces models were considered. However, C-doping –at other low coordinated sites– is not presented in extended models is even more favorable which shows the need to employ more realistic models for nanostructures involved in photocatalytic processes.

INTRODUCTION

Semiconducting photocatalysts have generated a great attention during last decades due to their potential applications in areas such as energy and environmental.[1,2] In particular, transition metal oxides (*i.e.*, TiO_2, ZnO, WO_3) and mixed oxides are the largest and most important families of photocatalytic materials.[3] Among them, titania (TiO_2) has gained much interest becoming in the workhorse in the field of heterogeneous photocatalysis.[4,5] This spotlight on TiO_2 is largely due to the seminal work of Fujishima and Honda, where the photolysis of water was electrochemically achieved using titania as semiconductor electrode under ultraviolet (UV) light.[6] From there the rise of water splitting for H_2 fuel generation using titania as photocatalyst has been meteoric.[7,8] However, the photocatalytic activity of TiO_2 remains still far from a horizon with commercial applications.[9,10]

The restrictive light absorption due to the large energy gap and the fast recombination of the photogenerated electrons and holes constitute the main limitations of photoactive TiO_2 derived nanostructures. Therefore, different strategies have been proposed to overcome such drawbacks, with the goal of improving the photocatalytic performance. These are, *i*) crystal facet engineering (*i.e.*, size, shape, and morphology of photoactive nanostructures),[11,12] *ii*) surface modification by supporting Pt, Pd or Ag nanoparticles,[13,14-15] *iii*) metal doping (*i.e.*, Fe, Co, Cr, Cu, and Au)[16,17-18] and non-metal doping (*i.e.*, C or N) doping,[19,20] *iv*) coupling TiO_2 with other semiconductors (*i.e.*, ZnO, WO_3 or CdS),[21,22] and *v*) the design of multiple components (*i.e.*, Ag-AgBr/TiO_2, Au-Pd/TiO_2 or Au-$SrTiO_3$/TiO_2).[23,24]

Here, we focus on non-metal elements, in particular C atoms, which inside the intrinsic TiO_2 structure minimize the restrictive light absorption either by reducing the energy gap or by creating intermediate energy levels between valence and conduction bands.[25] Hence, we pay attention to structural modifications with carbon (C-doped TiO_2). Experiments have confirmed the reason of visible light activity increasing of TiO_2 by the presence of C atoms in its atomic framework.[26,27] The presence of C atoms in the TiO_2 framework generates an interband C 2p states responsible for the energy gap narrowing. These electronic features were confirmed by the enhancing of C-doped TiO_2 photocatalytic degradation of organic compounds, even at low C concentration (*i.e.*, 1 wt%).[28,29-30]

The nature of carbon doping species has been experimentally analyzed through X-ray photoelectron (XPS) and infrared (IR) spectroscopies finding out substitutional carbon (replacing oxygen) and carbonate species. Instead of these great efforts, the atomic picture accessible through experiments is limited by technical aspects. Alternatively, computational techniques allow one obtaining valuable atomistic information, which can be used to rationalize the experimental observations.[31] In this context, Di Valentin *et al.*[32] investigated the modifications of carbon impurities varying the oxygen partial pressure on the electronic band structure of bulk titania polymorphs (*i.e.*, anatase and rutile) by using the density functional theory (DFT) method. The authors found that the substitution of O atoms by carbon (C_O) is thermodynamically favorable in an oxygen-poor atmosphere, whereas the substitution of Ti atoms by carbon (C_{Ti}) is preferential at oxygen-rich conditions. The former localizes states in the middle of energy gap, meanwhile the latter does not promote such reduction on the energy gap. Interestingly, C_{Ti} doping is energetically more favorable than C_O in anatase and rutile bulk systems. Additional studies over C-doped TiO_2 have been performed on the bronze (B) bulk titania phase.[33] This analysis suggested that the C_O doping is more favorable than C_{Ti}. Clearly, the atomic environment and structure of titania framework can play an important role in the stability of C-doping as shown by these studies which call for more detailed study. In part, this has been tackled recently by Curti *et al.* by analyzing C-doping in several surfaces and finding that C-doping on the (001) anatase surface is more favorable than on the (101) and (100) anatase surfaces.[34] While these studies provide useful insight, they considered C-doped anatase on extended models whereas the real systems involve finite nanoparticles. While periodic surfaces models are likely to accurately describe facet regions observed in nanostructures, there are other important regions such as corners or edges missed in such extended models. These regions featured in nanostructures can play a fundamental role when C-doped titania. The aim of the present study is to investigate the influence of C-doped on titania nanoparticles broadly investigated by some of us,[35,36] with the objective of fill the empty space in the state-of-the-art.

MODELS AND COMPUTATIONAL DETAILS

The doping by C atoms is investigated considering a realistic titania nanoparticle model. In particular, we selected the $(TiO_2)_{84}$ nanoparticle (NP) due to its realistic bipyramid morphology and realistic size (see Fig. 1).[37] It has been shown that this NP model belongs

to the so-called scalable regime at which the property scales towards the bulk.[38] Note that this bipyramidal model exposes the (101) surface on all facets of the NP. This configures stability to this morphology because the (101) surface is the most stable anatase surface thermodynamically speaking. Next, we selected different regions of the nanoparticle to introduce the C atom generating the doping of $(TiO_2)_{84}$ NP. These regions are O (C_O) and Ti (C_{Ti}) sites together to interstitial (C_i) regions.

To inspect the stability and electronic structure of the C-doped $(TiO_2)_{84}$ NP, we rely on density functional theory (DFT) based calculations carried out by explicitly including all electrons with the electron density described through a numerical atom-centered (NAO) orbital basis set as implemented in the Fritz Haber Institute *ab initio* molecular simulations (FHI-aims) code.[39] The generalized gradient approximation (GGA) such as PBE density functional was selected to describe the thermodynamic of the C-doped titania structures.[40] A light grid and tier-1 basis set was properly selected due to its numerical accuracy for TiO_2 systems similar to a valence triple zeta plus polarization Gaussian type orbitals (GTO) basis.[41] The convergence threshold for atomic forces in relaxation of all C-doped and pristine $(TiO_2)_{84}$ structures was set to 10^{-3} eV·Å^{-1}. Relativistic effects were included through the zero-order regular approach (ZORA)[42,43] because of the presence of Ti, a relatively heavy transition element. To overcome one of main drawback of the traditional density functional as PBE, namely its systematic underestimation of the energy gap of semiconducting materials,[44] more sophisticated density functionals based on hybrid technology are required. Thus, the hybrid PBEx density functional containing a 12.5% Fock exchange is able to describe quantitatively the band gap of stoichiometric and reduced rutile and anatase polymorphs[45] and anatase NPs,[46] was selected to provide a more accurate description picture of the molecular orbital energy level diagram of the C-doped TiO_2 NPs. Therefore, additional single point calculations were carried out for the PBE structures of the C-doped $(TiO_2)_{84}$ NP using the hybrid PBEx density functional with the aim of improving the quality of the Kohn-Sham energy levels.

The formation energy E_f for each doped nanoparticle is defined by:

$$E_f = E_{C@(TiO_2)_{84}} - E_{(TiO_2)_{84}} + \sum_i n_i \mu_i \quad (1)$$

where the total energy of doped and of pristine nanoparticles are described by $E_{C@(TiO_2)_{84}}$ and $E_{(TiO_2)_{84}}$, respectively. Eq. (1) is similar to the one used in previous works[32,47,48] but adapted to our NP models. Note that μ_i stands for the chemical potential of species *i* (*i.e.*,

Ti, O, and C), and n_i is the number of exchanged atoms by C atoms. We assume that $\mu_C = \mu_{CO_2} - \mu_{O_2}$, $\mu_{Ti} = \mu_{TiO_2} - 2\mu_O$, and $\mu_O = \frac{1}{2}E_{O_2} + \mu_O^{'}$ where $\mu_O^{'}$ takes values in the of -4 eV $\leq \mu_O^{'} \leq 0$ interval, to facilitate the comparison with previous studies.[32,34] The upper limit is the oxygen-rich conditions that is connected with experimental conditions. In particular, one may calculate the μ_O as a function of temperature and pressure; μ_O(700 K, 1 atm) = 0.723 eV. This value is translated into a very broad oxygen pressure interval of 6.5 10^{-48} atm $\leq P_{O_2} \leq 2.6 \cdot 10^{10}$ atm. For simplicity, and due the broad range of conditions explored, we neglect the vibrational contribution to the Gibbs free energy and thus μ_i of the rest of species can be replaced by total energies. We selected these conditions to perform a consistent and systematic comparison with previous results on anatase titania bulk and extended surfaces.[34]

The E_f for the three doping configurations: C_{Ti}, C_O, C_i, are calculated directly from the total energies of the doped nanoparticles as $E_{C@Ti_{83}O_{168}}$, $E_{C@Ti_{84}O_{167}}$, and $E_{C@Ti_{84}O_{168}}$ respectively.

$$E_{f,C_{Ti}}(700\ \text{K}, P) = E_{C@Ti_{83}O_{168}} + E_{TiO_2} - E_{Ti_{84}O_{168}} - E_{CO_2} - 2\mu_O^{'}(700\ \text{K}, P) \quad (2)$$

$$E_{f,C_O}(700\ \text{K}, P) = E_{C@Ti_{84}O_{167}} + \frac{3}{2}E_{O_2} - E_{Ti_{84}O_{168}} - E_{CO_2} + \mu_O^{'}(700\ \text{K}, P) \quad (3)$$

$$E_{f,C_i}(700\ \text{K}, P) = E_{C@Ti_{84}O_{168}} + E_{O_2} - E_{Ti_{84}O_{168}} - E_{CO_2} \quad (4)$$

where E_{TiO_2} and $E_{Ti_{84}O_{168}}$ are the total energy of one TiO_2 unit in gas phase and the total energy of the titania nanoparticle composed by 84 TiO_2 units. Finally, E_{CO_2} and E_{O_2} represent the total energy of the CO_2 and O_2 molecules. Note that the latter is the total energy of the triplet state, the ground state electronic configuration for the O_2 molecule.

RESULTS AND DISCUSSION

In this section the formation energy of C_O, C_{Ti} and C_i is described following the above mentioned eqs. (2-4). This will allow us identifying the most suitable sites for the doping of the $(TiO_2)_{84}$ NP and more importantly identify the preferential type (*i.e.*, by substituting Ti or O by C atoms, or locating C in an interstitial region). Finally, we analyse the impact of such doping on the resulting energy gap of the doped $(TiO_2)_{84}$ NPs and

compare to previous results for C-doped bulk[32] anatase and for the previously reported surfaces.[34]

We start with the C-doped $(TiO_2)_{84}$ by considering O substitution by C on the sites where, in terms of energy, oxygen vacancies are most likely to be formed.[49] Using the PBE density functional, a total of six different sites were analysed in previous work[49] featuring O vacancy formation energy in the 3.63 - 4.54 eV range. These sites involve O at the apical (or top), edge, facet and inside regions and, thus, the capital letters T, E, F and I were employed as notation to distinguish them. To complete the notation, the capital letter is accompanied by digits to different the sites located in the same region of the nanoparticle, see Fig. 2. The all set of sites is depicted in Fig. S1 in the ESI.

Fig. 3 shows the evolution of E_{f,C_O} at temperature of 700 K as a function of the oxygen chemical potential. The formation of C-doped structures by substituting C by O atoms is more favorable at oxygen-poor conditions ($\mu_O^{'}$ = -4 eV) and losses stability as moving toward oxygen-rich conditions ($\mu_O^{'}$ = 0 eV). This trend is systematically observed regardless the doping site. The doping site located inside of the $(TiO_2)_{84}$ framework and labeled as I-3-1 emerges as the most suitable site for the C_O doping whereas the C-doped in the apical region (T-1) is energetically the most unfavorable in all range of the oxygen chemical potential. The rest of sites are located somewhere in the middle. The C_O doping in facet regions, F-2 and F-3, are competitive. On the other hand, the C_O doping in edge region (E-2) is slightly more favorable than in facet ones. Finally, the doping in the I-3-2 is the second site unfavorable below T-1 site. In short, C_O doping is favorable at oxygen-poor conditions ranging the E_{f,C_O} 6.6 and 9.1 eV. Previous studies on anatase surface models reported E_{f,C_O} slightly above 8 eV at similar thermodynamic conditions.[34] Considering that in surface models the preferential region is facet, our results are consistent because the F-2 and F-3 exposed E_{f,C_O} around 8 eV.

Next, we analyze the formation energy of C-doped structures when substituting Ti atoms ($E_{f,C_{Ti}}$). These structural modifications are denoted as C_{Ti}. Noting that the two pyramids of the $(TiO_2)_{84}$ NP are rotated by 90 degrees and connected by their square base. Investigating the Ti atoms located in a quarter of one pyramid is enough to obtain a representative landscape of $E_{f,C_{Ti}}$ due to symmetrical reasons. Similar notation of the C_O is employed (*i.e.*, E, F, I, and T for edge, facet, inside, and top sites) followed by digits. These start with digit 1 for the sites located in the apical region and it progressively increases when C_{Ti} moving far away apical towards equatorial region (see Fig. S2 of ESI).

Fig. 4 shows the evolution of $E_{f,C_{Ti}}$ with the oxygen chemical potential. Contrary to E_{f,C_O}, the formation of C-doped titania at Ti sites (see Fig. S2) is energetically unfavorable at oxygen-poor conditions requiring energy above 12 eV. However, it starts to be favorable when moving towards oxygen-rich condition where $E_{f,C_{Ti}}$ is in the range of 4–8 eV. Focusing on this condition, we see that the C_{Ti} in T-1 is the most favorable to form. This is not surprising because the resulting C-doped structure forms a planar carbonate unit (CO_3) in the apical region. Similar situation is observed in the edge regions. Facet regions are less favorable. In short, the sites labeled as T-1, E-2 and E-3 emerges as the most preferential sites to form C_{Ti} (see Fig. 2). The formation of C_{Ti} in $(TiO_2)_{84}$ NP is energetically less favorable than on the (101), (100) and (001) anatase surfaces.[34] From and formation energy viewpoint, C_{Ti} in $(TiO_2)_{84}$ NP is similar to C_{Ti} in anatase bulk phase. Instead of these differences, the C atom trends to stabilize at the C_{Ti} site located closer to the surface, which is consistent with our results that are preferential in apical and edge regions.

The third region investigated to form C-doped $(TiO_2)_{84}$ nanostructures is the interstitial (C_i), which is unaltered by oxygen chemical potential as defined in eq. (4). The interstitial sites are located inside the titania nanoparticle and, thus, only the I capital letter is used in the notation followed by three digits (see Fig. S3). The first one indicates its position respect to the apical region like the C_{Ti} notation, meanwhile the second one indicates the interstitial channel and third, the position inside the interstitial channel. In general, E_{f,C_i} takes values around 8.5 eV (Fig. 5). The formation of this C_i defect is energetically more favorable than on bulk (~11 eV).[34]

Finally, a general view about the C-doped $(TiO_2)_{84}$ NP is depicted in Fig. 5 by analyzing exclusively the C_O, C_{Ti}, and C_i with the lowest formation energies as shown in Fig. 2. There are two regions well defined, i) oxygen-poor region, where C_O doping is the most favorable, and ii) oxygen-rich region, where the C_{Ti} are the most plausible sites for C-doped $(TiO_2)_{84}$ according to our predictions. More interestingly is the region where $\mu_O^{'}$ is equal to -2 eV. Here, it appears several crossovers among all doping sites indicating that the C-doped $(TiO_2)_{84}$ may be competitive and very sensible to small variations of $\mu_O^{'}$. Our trends of each C-doped at oxygen and titanium sites are similar to previous results reported in bulk anatase.[34] However, C_{Ti} is energetically favorable in all range of $\mu_O^{'}$ and this is not the case found in C-doped $(TiO_2)_{84}$ NP as mentioned. This comparison justifies the importance of selected realistic titania when describing doping titania systems. In part,

because our results go well beyond this picture because include several sites and regions found in finite nanostructure model as $(TiO_2)_{84}$ that are not present in bulk or extended surface models.

The main objective of non-metal doping of semiconducting oxides is to reduce the energy gap observed in the undoped structure. Therefore, we now analyze the electronic properties of C-doped $(TiO_2)_{84}$ NP focusing on the distribution of the Kohn-Sham orbital energies which, even if rigorously speaking do not coincide with the quasiparticle energies, are able to provide qualitative trends. We exclusively analyze the most suitable C-doped structure depicted in Fig. 2. To overcome the systematic underestimation of the energy gap of semiconducting materials by standard GGA functionals,[44] we perform additional calculations using the hybrid PBEx density functional. Bare $(TiO_2)_{84}$ NP has an energy gap of 2.52 eV with PBE density functional and it opens to 3.60 eV with PBEx density functional. Fig. 6 shows the Kohn-Sham orbital energies of all C-doped situations together with bare $(TiO_2)_{84}$ NP. Clearly, the inclusion of C-doped alters mainly the highest occupied molecular orbital (HOMO) whereas the lowest unoccupied one (LUMO) appears to be unaltered instead of the significant structural modification. C-doping at oxygen and interstitial sites promote the reduction of the energy gap improving in principle the photoactivation of the titania nanoparticle in the VIS region. On the other hand, we find that C-doping at titanium sites has a negligible influence on the resulting energy gap, which is similar to that observed in the undoped situation. In short, C_{Ti} is not visible-light-active even though it is the most stable under ambient oxygen conditions.

CONCLUSIONS

To analyze the effect of C-doping on anatase beyond periodic models for bulk or extended surfaces, the $(TiO_2)_{84}$ NP is selected as representative of those in the scalable regime. Three different regions are considered to locate the carbon atom in the structural framework of the nanoparticle. We considered oxygen, titanium, and interstitial sites labeled as C_O, C_{Ti} and C_i, respectively. Taking the formation energy (E_f) as descriptor to identify the most suitable sites for C-doped $(TiO_2)_{84}$ NP, the most favorable region to form C-doped structure by substituting O per C atom is inside the nanoparticle (I-3-1). On the other hand, facet sites (F-2 and F-3) shown formation energy in agreement with the findings reported in previous work using extended models[34] and thus validates, in part, their predictions. However, the apical region (T-1) is the most favorable to form C-doped structure by switching Ti per C atom, a situation which cannot be represented by

bulk and surface models. In this latter case, the formation of planar carbonate species (CO_3) is an indicator that confirm such stability. Nevertheless, the two situations described above are energetically favorable in all range of μ_O'. In general, the C_O formation energy destabilizes as increasing μ_O', meanwhile C_{Ti} stabilizes with increasing μ_O'. Finally, C_i is non-dependent of μ_O' and its value is constant along the range of μ_O'. In short, C_O (I-3-1) is stable in $-4 \leq \mu_O' \leq -2.2$ eV; C_i (I-3-2-3) is in $-2.2 \leq \mu_O' \leq -1.9$ eV; and finally, C_{Ti} (T-1) is the most stable in the range of $-1.9 \leq \mu_O' \leq 0$ eV. This confirms that the oxygen atmosphere is a fundamental parameter to control the sites where the formation of C-doped structures takes place. This scenario is completely different to that observed in anatase bulk phase where C_{Ti} is stable along the range of μ_O'.[34]

The analysis of the Kohn-Sham energy orbitals confirms the reduction of energy gap of C-doped $(TiO_2)_{84}$ NP respect to its bare configuration. The E_{gap} is reduced when carbon atoms occupy oxygen sites (C_O) or interstitial sites (C_i). This is due to carbon atoms introduce additional energy levels between the HOMO and LUMO of $(TiO_2)_{84}$ NP. The case of C_{Ti} unalters the Kohn-Sham energy orbitals and there is no changes respect to the bare $(TiO_2)_{84}$ NP. This behavior was consistently observed in bulk anatase phase.[32] In short, C-doped $(TiO_2)_{84}$ NPs could be active by VIS light at low oxygen partial pressures where substitution at oxygen sites and interstitial regions are feasible for hosting carbon atoms.

To summarize, the $(TiO_2)_{84}$ NP includes new sites for C-doping titania due to the presence of sites and regions not found in extended models some of which are more favorable than the corresponding ones in bulk and surface models. The present work indicates that to reach a more accurate picture of nonmetal and metal doping in photoactive materials it is necessary to beyond bulk and surface periodic models. It is likely that the present results hold for other photoactive materials beyond titania.

ACKNOWLEDGEMENTS

The authors thank Prof. Dr. Francesc Illas for his useful discussions during the development of this investigation. This study has been supported by the Spanish MICIN PID2020-115293RJ-I00/AEI/10.13039/501100011033, MICIN/FEDER RTI2018-095460-B-I00 /AEI/10.13039/501100011033 projects and María de Maeztu MDM-2017-

0767 grant. The authors also thank the COST Action 18234 supported by the European Cooperation in Science and Technology (COST).

Fig. 1. Side and top views of $(TiO_2)_{84}$ NP. This nanostructure exposes a bipyramidal morphology and exposed the (101) surfaces in eight facets of the nanoparticle. Red and blue spheres correspond to oxygen and titanium atoms.

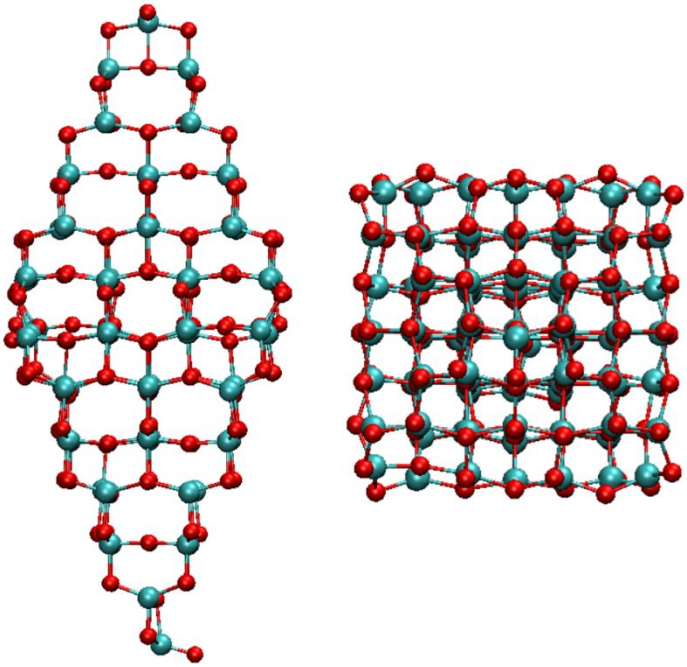

Fig. 2 Side and top views of the representative optimized C-doped $(TiO_2)_{84}$ NPs at O (C_O), Ti (C_{Ti}) and interstitial (C_i) sites. Blue, red, and black spheres denote titanium, oxygen, and carbon, respectively. Note that C-atom have been represented with double radius to show clearly doping site.

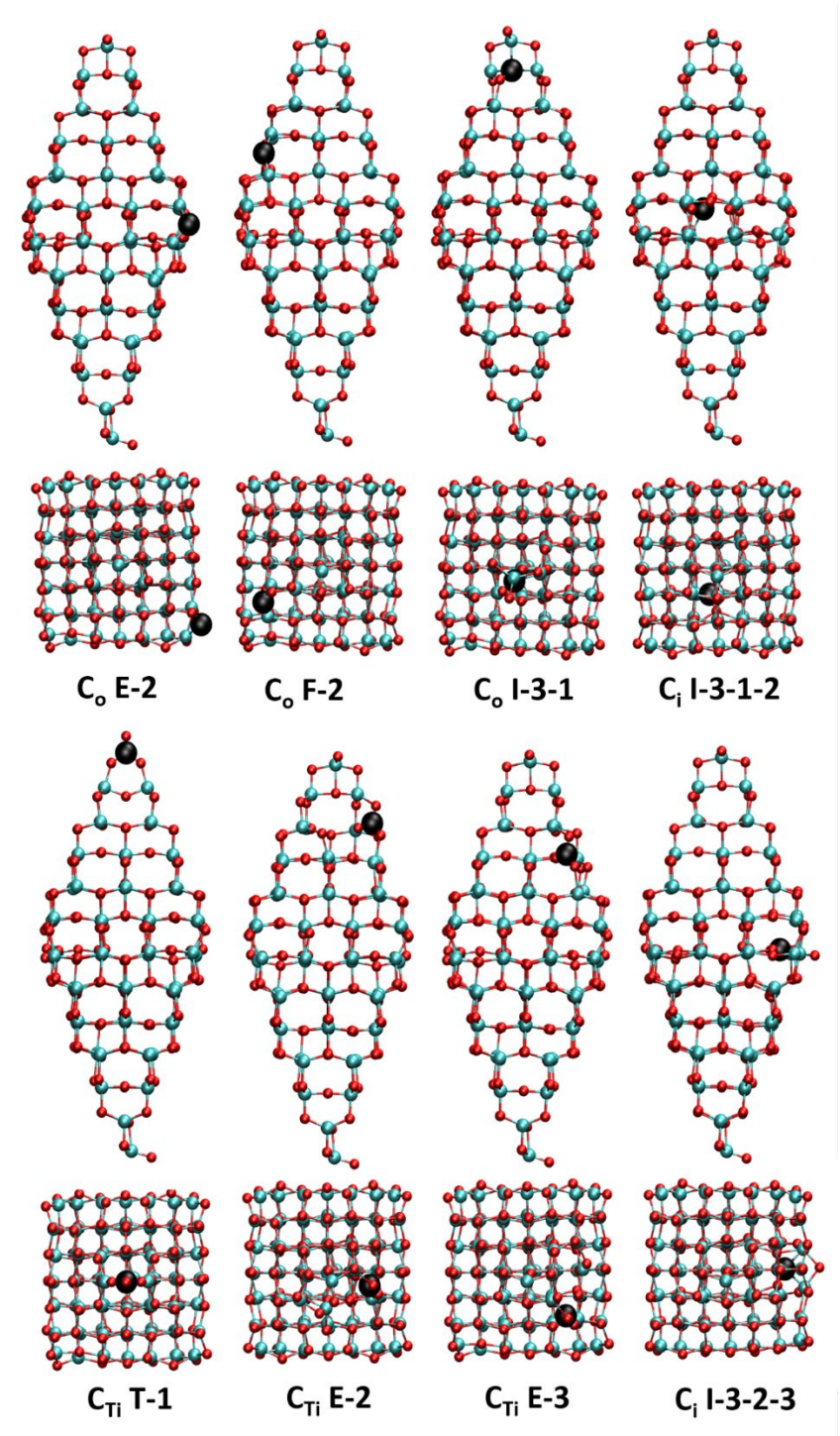

Fig. 3 Formation energies (E_{f,C_O}, in eV) as a function of the oxygen chemical potential (μ_O') for different C_O carbon species in $(TiO_2)_{84}$ NP.

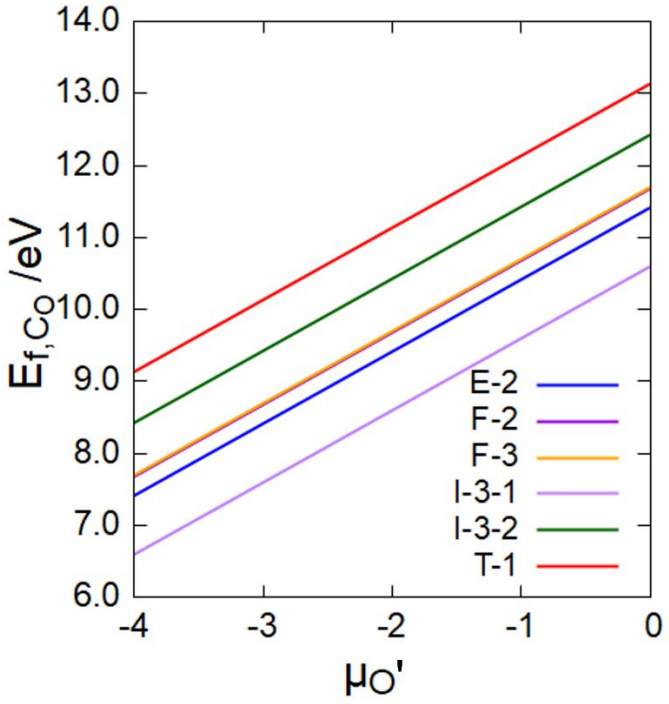

Fig. 4 Formation energies ($E_{f,C_{Ti}}$, in eV) as a function of the oxygen chemical potential (μ_O') for different C_{Ti} carbon species in $(TiO_2)_{84}$ NP. Colour code: blue line, T-1; violet line, edged position (E-1, E-2, E-3, E-4, E-5, E-6); orange line, face position (F-1, F-2, F-3, F-4) and green line, internal position (I-2, I-3).

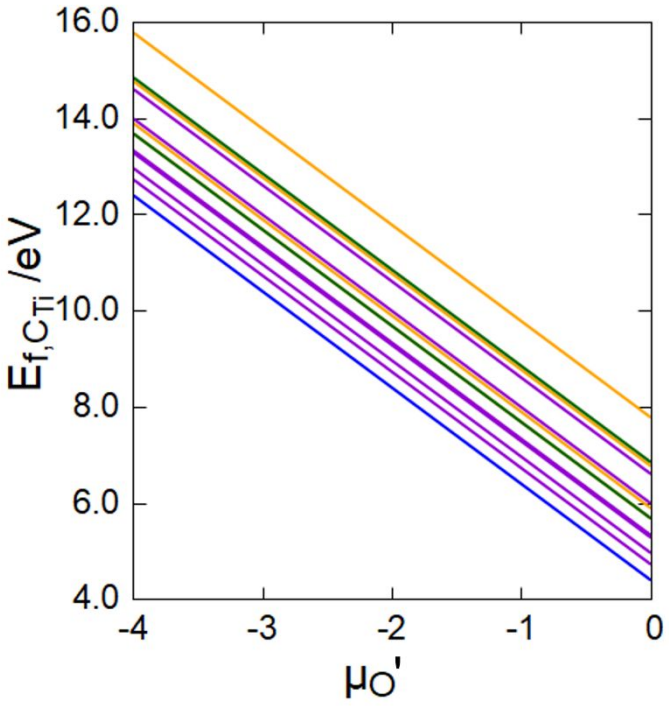

Fig. 5 Formation energies $E_{f,C_{Ti}}$, E_{f,C_O} and E_{f,C_i} in eV as a function of the oxygen chemical potential (μ_O') for different C_{Ti} , C_O and C_i doped $(TiO_2)_{84}$ NP.

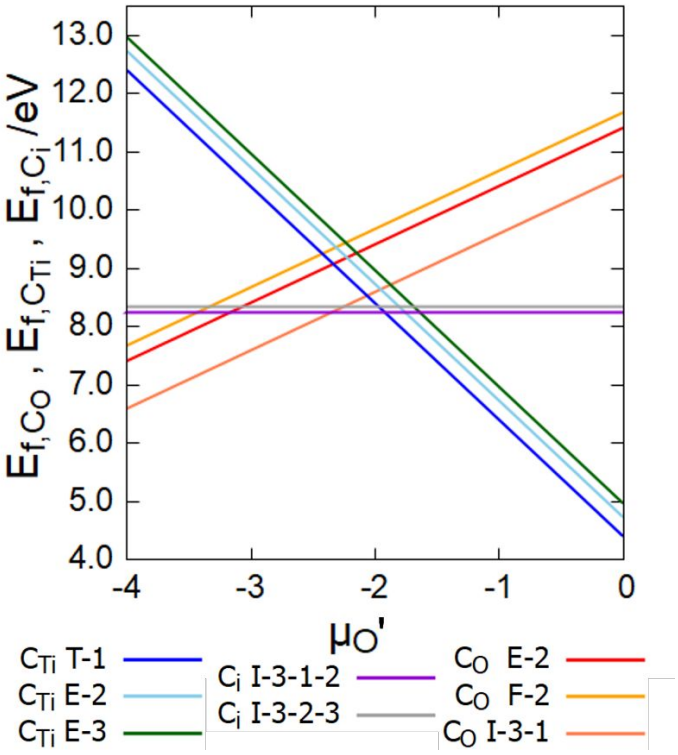

Fig. 6 Kohn-Sham orbital energy level diagram of $(TiO_2)_{84}$ NP and C-doped $(TiO_2)_{84}$ NPs as predicted from DFT based calculations with the PBEx functional. The red dotted lines correspond to the standard redox potentials for water splitting at pH = 0 (H^+/H_2 = -4.44 eV and O_2/H_2O = -5.67 eV).

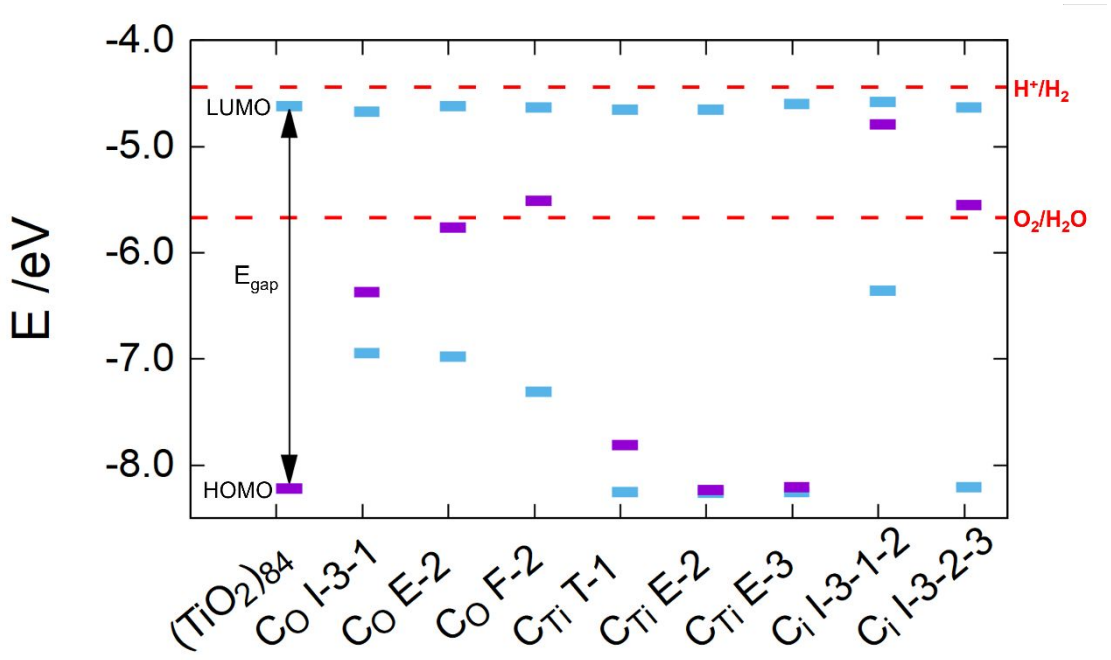

REFERENCES

(1) N. Serpone and A. V. Emeline, *J. Phys. Chem. Lett.*, 2012, **3**, 673-677.

(2) L. Zhang, J. Ran, S.-Z. Qiao and M. Jaroniec, *Chem. Soc. Rev.*, 2019, **48**, 5184-5206.

(3) C. Karthikeyan, P. arunachalam, K. Ramachandran, A. M. Al-Mayouf and S. Karuppuchamy, *J. Alloys Comp.*, 2020, **828**, 154281.

(4) A. L. Linsebigler, G. Lu and J. T. Yates Jr., *Chem. Rev.*, 1995, **95**,735-758.

(5) J. Schneider, M. Matsuoka, M, Takeuchi, J. Zhang, Y. Horiuchi, M. Anpo and D. W. Bahnemann, *Chem. Rev.*, 2014, **114**, 9919-9986.

(6) A. Fujishima and K. Honda, *Nature*, 1972, **238**, 37-38.

(7) K. Maeda and K. Domen, *J. Phys. Chem. Lett.*, 2010, **1**, 2655-2661.

(8) T. Takata, J. Jiang, Y. Sakata, M. Nakabayashi, N. Shibata, V. Nandal, K. Seki, T. Hisatomi and K. Domen, *Nature*, 2020, **581**, 411-414.

(9) K. Villa, J. R. Galán-Mascarós, N. López and E. Palomares, *Sustainable Energy Fuels*, 2021, **5**, 4560-4569.

(10) M. Melchionna and P. Fornasiero, *ACS Catal.*, 2020, **10**, 5493-5501.

(11) G. Liu, J. C. Yu, G. Q. Lu and H.-M. Cheng, *Chem. Commun.*, 2011, **47**, 6763-6783.

(12) S. Wang, G. Liu and L. Wang, *Chem. Rev.*, 2019, **119**, 5192-5247.

(13) M. Batzill, *Energy Environ. Sci.*, 2011, **4**, 3275-3286.

(14) J. Low, B. Cheng and J. Yu, *Appl. Surf. Sci.*, 2017, **392**, 658-686.

(15) B. Nandi, R. Uppaluri and M. Purkait, *J. Membr. Sci.*, 2009, **330**, 246-258.

(16) W. Choi, A. Termin and M. R. Hoffmann, *J. Phys. Chem.*, 1994, **98**, 13669-13679.

(17) J. Chen, F. Qiu, W. Xu, S. Cao and H. Zhu, *Appl. Catal. A*, 2015, **495**, 131-140.

(18) J. Cai, J. Huang and Y. Lai, *J. Mater. Chem. A*, 2017, **5**, 16412-16421.

(19) X. Chen and C. Burda, *J. Am. Chem. Soc.*, 2008, **130**, 5018-5019.

(20) T. Ohno, T. Mitsui and M. Matsumura, *Chem. Lett.*, 2003, **32**, 364-365.

(21) H. Wang, L. Zhang, Z. Chen, J. Hu, S. Li, Z. Wang, J. Liu and X. Wang, *Chem. Soc. Rev.*, 2014, **43**, 5234-5244.

(22) D. Robert, *Catal. Today*, 2007, **122**, 20-26.

(23) H. Zhou, Y. Qu, T. Zeid and X. Duan, *Energy Environ. Sci.*, 2012, **5**, 6732-6743.

(24) M. Wang, D. Zheng, M. Ye, C. Zhang, B. Xu, C. Lin, L. Sun and Z. Lin, *Small*, 2015, **11**, 1436-1442.

(25) Y. Cong, J. Zhang, F. Chen and M. Anpo, *J. Phys. Chem. C*, 2007, **111**, 6976-6982.

(26) H. Kisch and W. Macyk, *ChemPhysChem*, 2022, **3**, 399-400.

(27) V. Etacheri, G. Michlits, M. K. Seery, S. J. Hinder and S. C. Pillai, *ACS Appl. Mater. Interfaces*, 2013, **5**, 1663-1672.

(28) J. Matos, J. Ocares-Riquelme, P. S. Poon, R. Montaña, X. García, K. Campos, J. C. Hernández-Garrido and M. M. Titirici, *J. Coll. Inter. Sci.*, 2019, **547**, 14-29.

(29) C. H. Chiou, C. Y. Wu and R. S. Juang, *J. Chem. Eng.*, 2008, **139**, 322-329.

(30) Y. Cheng, H. Sun, W. Jin and N. Xu, *Chem. Eng. J.*, 2007, **128**, 127-133.

(31) B. Samanta, Á. Morales-García, F. Illas, N. Goga, J. A. Anta, S. Calero, A. Bieberle-Hütter, F. Libisch, A. B. Muñoz-García, M. Pavone and M. C. Toroker. *Chem. Soc Rev.*, 2022, **52**, 3794-3818.

(32) C. Di Valentin, G. Pacchioni and A. Selloni, *Chem. Mater.*, 2005, **17**, 6656-6665.

(33) H. Heffner, R. Faccio and I. López-Corral, *Appl. Surf. Sci.*, 2021, **551**, 149479.

(34) M. Curti, C. B. Mendive, T. Bredow and D. W. Bahnemann, *J. Phys. Chem. C*, 2021, **125**, 24263-24272.

(35) Á. Morales-García, A. M. Escatllar, F. Illas and S. T. Bromley, *Nanoscale*, 2019, **11**, 9032-9041.

(36) L. Mino, Á. Morales-García, S. T. Bromley and F. Illas, *Nanoscale*, 2021, **13**, 6577-6585.

(37) M. Cargnello, T. R. Gordon and C. B. Murray, *Chem. Rev.*, 2014, **114**, 9319-9345.

(38) S. T. Bromley, I. de P. R. Moreira, K. M. Neyman and F. Illas, Chem. Soc. Rev., 2009, **38**, 2657-2670

(39) V. Blum, R. Gehrke, P. Hanke, P. Havu, V. Havu, X. Ren, K. Reuter and M. Scheffler, *Comput. Phys. Commun.*, 2009, **180**, 2175-2196.

(40) J. P. Perdew, K. Burke and M. Ernzerhof, *Phys. Rev. Lett.*, 1996, **77**, 3865-3868.

(41) O. Lamiel-García, K. C. Ko, J. Y. Lee, S. T. Bromley and F. Illas, *J. Chem. Theory Comput.*, 2017, **13**, 1785-1793.

(42) C. Chang, M. Pelissier and M. Durand, *Phys. Scr.*, 1986, **34**, 394-404.

(43) E. van Lenthe, R. van Leeuwen, E. J. Baerends and J. G. Snijders, *Int. Quantum Chem.*, 1994, **57**, 281-293.

(44) Á. Morales-García, R. Valero and F. Illas, *J. Phys. Chem. C*, 2017, **121**, 18862-18866.

(45) K. C. Ko, O. Lamiel-García, J. Y. Lee and F. Illas, *Phys. Chem. Chem. Phys.*, 2016, **18**, 12357-12367.

(46) Á. Morales-García, R. Valero, F. Illas, *Phys. Chem. Chem. Phys.*, 2018, **20**, 18907-18911.

(47) Y. Y. Sun and S. Zhang, *Phys. Chem. Chem. Phys.*, 2016, **18**, 2776-2783.

(48) K. Reuter and M. Scheffler, *Phys. Rev. B*, 2001, **65**, 035406.

(49) Á. Morales-García, O. Lamiel-García, R. Valero and F. Illas, *J. Phys. Chem. C* 2018, **122**, 2413−2421.

TOC